Module 4: Interferometry

Lecture 24: Iterative algorithms

The Lecture Contains:

Previous Next

MART

When the correction in the iterative algorithms are multiplicative rather than additive, the algorithms are grouped under the family of MART (Verhoeven, [311]). Gordon et al. [97] and Gordon and Herman [100] have suggested different forms of MART. The MART algorithms presented below are similar to those considered by Verhoeven [31].

The major difference between ART and MART algorithms is in the method of computing the corrections. While ART uses the difference between the calculated projections and measured projections, MART uses the ratio between the two. Hence the corrections applied to each cell during calculations are via the multiplication operation. The structure otherwise is similar to Gordon's ART (ART2).

The individual steps of three versions of MART (1,2, and3) are summarized below.
start: 1start iterations (k):
start: 2 For each projection angle (θ):
start: 3 For each ray $(i\theta)$:
Compute the numerical projection
Calculate the correction as:

$$\Delta\phi_{i\theta} = \frac{\phi_{i\theta}}{\tilde{\phi}_{i\theta}}$$

Start: 4 For each cell (j):

If $w_{i\theta,j}$ is non-zero then:
MART1:

$$f_j^{\text{new}} = f_j^{\text{old}} \times \left(1.0 - \mu \times (\Delta\phi_{i\theta})\right)$$

MART2:

$$f_j^{\text{new}} = f_j^{\text{old}} \times \left(1.0 - \mu \times \frac{w_{i\theta,j}}{(w_{i\theta,j})_{\max}} \times (1.0 - \Delta\phi_{i\theta})\right)$$

MART3:

$$f_j^{\text{new}} = f_j^{\text{old}} \times (\Delta\phi_{i\theta}) \frac{\mu\, w_{i\theta,j}}{(w_{i\theta,j})_{\max}}$$

where μ is a relaxation factor.

close: 4
close: 3
close: 2
Check for convergence as:
If

$$abs\left[\frac{f^{k+1}-f^{k}}{f^{k+1}}\right]\times 100 \leq e$$

where e is a suitable stopping criterion.
STOP:
Else: Continue
close: 1

Steps 3 and 4 form the essence of the reconstruction algorithm. All three versions include the relaxation factor μ. Typical values of the relaxation factor reported are in the range 0.1 - 1.0, larger values leading to divergence It is to be noted that the correction calculated in step 3 is the ratio of the recorded projection data ($\phi_{i\theta}$) and that calculated from the guessed field, namely $\widetilde{\phi_{i\theta}}$ which is being iterated. The three versions of MART differ in the manner in which the corrections are implemented. In MART 1. The weight function is prescribed in binary form, being unity if a particular ray passes through a pixel and zero otherwise . In MART 2 and MART 3, the weight function is precisely calculated as the ratio of the length of the ray intercepted by the pixel and the maximum dimension of a segment enclosed by it.

Previous Next

AVMART

The reconstruction of a function from a finite number of projections recorded at different view angles leads to an ill-posed matrix inversion problem. The problem is accentuated when the projection data is limited. The resulting matrix is rectangular with the number of unknowns being greater than the number of equations. In view of the ill-conditioning of the matrix, the convergence of the matrix, the convergence of the iterations to any particular solution is dependent on the initial on the initial guess, the noise level in the projection data and the under-relaxation parameter employed. In the present study, the MART algorithm has been extended so as to

- enlarge the range of the usable relaxation factor.
- diminish the influence of noise in the projection data, and
- guarantee a meaningful solution when the initial guess is simply a constant.

The original MART algorithm described above has been modified in the present work to form a new approach to applying the corrections. In the proposed algorithm the corrections are calculated by considering all the rays from all the angles passing through a given pixel. Instead of a single correction obtained from individual rays, a correction that is determined as determined as the average of all the rays is used. The difference between the conventional MART and the present implementation is the following. The correction at each pixel is updated on the basis of the N-th root of the product of all the corrections from all the *N* rays of all view angles passing through a pixel. This idea is based on the fact that average corrections are expected to behave better in the presence of noisy projection data. Since an average correction is introduction, the algorithm is desensitized to noise. There is however a potential drawback. Since an average pixel correction based on a set of rays is computed, the reconstructed field is not required to satisfy exactly the recorded projection data. This was seen to be no cause for concern for the three application considered. The projection data was exactly satisfied by the reconstructed field in each case.
The modified algorithms have been identified below as AVMART, The prefix AV referring to average. The important step, namely step 4 alone is presented here, with the understanding that all other steps remain unchanged.

Start: 4 For each cell (j):
Identify all the rays passing through a given cell (j): Let be the total number of rays passing through the j- th cell.
Apply correction as:

AVMART1:

$$f_j^{new} = f_j^{old} \times \left(\prod_{Mcj} (1.0 - \mu \times (\Delta\phi_{i\theta})) \right)^{\frac{1}{Mcj}}$$

AVMART2:

$$f_j^{new} = f_j^{old} \times \left(\prod_{Mc_j} \left(1.0 - \mu \times \frac{w_{i\theta,j}}{(w_{i\theta,j})_{max}} \times (1.0 - \Delta\phi_{i\theta}) \right) \right)^{\frac{1}{Mc_j}}$$

AVMART3:

$$f_j^{new} = f_j^{old} \times \left(\prod_{Mc_j} (\Delta\phi_{i\theta})^{\frac{\mu w_{i\theta,j}}{(w_{i\theta,j})_{max}}} \right)^{\frac{1}{Mc_j}}$$

Close:4

The symbol $\prod$ in the three algorithms above represents a product over the variable Mc_j. The Mc_j-th root of this product is evaluated in each approach. The relaxation factor has been retained in the statements above for completeness. In all calculations, it was set equal to unity to bring out a mixture of the “smooth “ and “sharp” features of the temperature field. The proposed algorithms require a smaller CPU time per iteration, when compared to the existing ones, Section 6.7 evaluates the benefits derived by modifying step 4 for problems of practical importance.

Previous Next

Maximum Entropy

Based on ideas from information theory, one can perform image analysis and construct meaningful tomographic algorithms, algorithms. Suppose there is a source which generates a discrete set of independent messages r_k with probabilities p_k. Then the information associated with r_k is defined logarithmically as

$$I_k = -\ln P_k$$

The entropy of the source is defined as the average information generated generated by the source and can be calculated as

$$\text{entrophy} = -\sum_{k=1}^{L} P_k \ln P_k$$

When the source is the image, the probability can be replaced by the gray level f_j, for the j −th pixel and entropy can be redefined as

$$\text{entrophy} = -\sum_{j=1}^{N} f_j \ln f_j$$

For natural systems, the organization of intensities f_j, over the image can be expected to follow the second law of thermodynamics namely,

$$f_j : -\sum_{j} f_j \ln f_j = \text{maximum}$$

This is the basis of the MAXENT algorithm. For interferometric images, one can view the pixel temperature as the information content and entropy built up using their magnitudes. In the absence of any constraint, the solution of the above optimization problem will correspond to a constant temperature distribution, more generally a uniform histogram in terms of probabilities. Hence, the MAXENT algorithm is properly posed only along with the projections as constraints.

Requiring that the entropy of the system be a maximum along with the interferometric projections as constraints is known as the Maximum entropy optimization technique (MAXENT). It produces an unbiased solution and is maximally noncommittal about the unmeasured parameters. This technique is particularly attractive when the projection data is incomplete. The MAXENT algorithm is described below:

Consider a continuous function (x, y, z) with condition $(x, y, z) \geq 0$ and values $f_j \text{at } j = \cdots N$ pixels. In the present context, the entropy technique refers to the extermination of the

$$F = -\sum_{j=1}^{N} f_j \ln|f_j| \qquad (23)$$

Subject to a set of constraints. In constraints. In MAXENT the collected projection data and any other

a priori information about the field to be reconstructed can be viewed as the constraints over which the entropy is to be maximized. A typical maximum entropy problem can be stated as:

$$\text{Maximize}\left(-\sum_{j=1}^{N} f_j^2\right)$$

$$\text{subject to } \phi_j = \sum_{j=1}^{N} w_{ij} f_i \qquad (24)$$

$$\text{and } f_j \geq 0$$

Different schemes are available for optimizing a function over some constraints, for example the Lagrange multiplier technique. The MART algorithms have been shown to be equivalent to the maximum entropy algorithm in the literature. Hence the entropy algorithm has not been considered further in the present article.

Previous Next

Minimum Energy

The MAXENT algorithm can be generalized for any other fumction in place of entropy. Gull and Newton [30] have suggested four such functions which can be maximized with the projections as constraints to obtain the tomographic reconstruction. After entropy, the energy functions are attractive and natural for use in physical problems. The minimum energy method (MEM) can be implemented in a manner analogous to MAXENT as follows

$$\text{Maximize}\left(-\sum_{j=1}^{N} f_j^2\right) \qquad (25)$$

$$\text{subject to } \phi_j = \sum_{j=1}^{N} w_{ij} f_i$$

Compared to MAXEMT, MEM has a simper implementation while using the Lagrangian multiplier technique, since it results in a set of linear equations. Gull and Newton however have recommended the MAXENT over MED, since they found that the MEM produces a field which is negatively correlated and hence produced a biased solution.

Previous Next

Testing of Tomographic Algorithms

The ART, MART and the optimization algorithms have been for variety of cases by subbarao et al. [32]. In the examples, the temperature fields were synthetically generated. Hence it was possible to determine explicitly the convergence properties and errors for each of the methods. Among the various algorithms, the authors have identiflied MART3 as the best in terms of the error and CPU time requirements. The AVMART algorithms proposed by the author and his coworkers have been validated in the present section against two benchmark cases (1) a circular region with five holes, and (2) the numerically generated three-dimensional temperature field in fluid convection. Employing a temperature field similar to that encountered in the experiments aids in the choice of the proper initial guess and error levels to be anticipated. This also helps in selecting the proper tomographic algorithm. The algorithms stated in Sections MART and AVMART have been rested for a circular region with distribution of holes and a numerically generated three-dimensional temperature field in Rayleigh-Benard convection. Sensitivity of the algorithms to noise has been tested in the context of numerically generated temperature data. Issues addressed in the sensitivity study are initial guess, noise in projection data, and the effect of increasing number of projections on the accuracy of reconstruction.

Reconstruction of a Circular Disk with Holes

A circular region with five symmetrically placed holes is considered. The object is recognized in terms of the local dimensionless density, which is zero at the holes and unity elsewhere. To implement the reconstruction algorithm, it is convenient to enclose the circular object within a square domain. The gap between the circle and the square is specified to have zero density (in calculations, a value of 0.001 has been used for zero density). The square region is discredited into 61×61 cells in the x and y directions. Projections of this object have been determined analytically and hence exact. The recovery of the original object from a limited number of these projections using the original MART as well as the proposed AVMART algorithms is discussed below.

Projections at angles of 0, 45, 90,and 135 degrees have been considered in the present application. The initial guess for the density field was a constant value of unity. A convergence criterion of 1% for the iterations has been uniformly used. At a Convergence of 0.01% , the solution was practically identical, except that errors were seen to be marginally higher. This feature of topographic algorithms, that convergence is asymptotic (but not monotonic) has been reported earlier. Such trends are to be expected in the reconstruction of fields having a step discontinuity. At the hole boundary in the present example. The relaxation factor was set at 0.1in case of original MART while it was unity in the AVMART algorithms. All calculations were carried out on a DEC–alpha workstation with 196 MB RAM and a 223 MHz processor.

A summary of the reconstructed fields using the three original and three proposed algorithms is shown in Fields 33. In principle, all the six algorithms were seen to converge to a qualitatively meaningful solution. The void fraction, namely the fraction of the space occupied by the holes was 0.34 in the present application. In the reconstructed solution, the void fraction can be determined from the formula

$$\text{void fraction} = 1.0 - \frac{\sum_{i=1}^{N} \rho_i}{N}$$

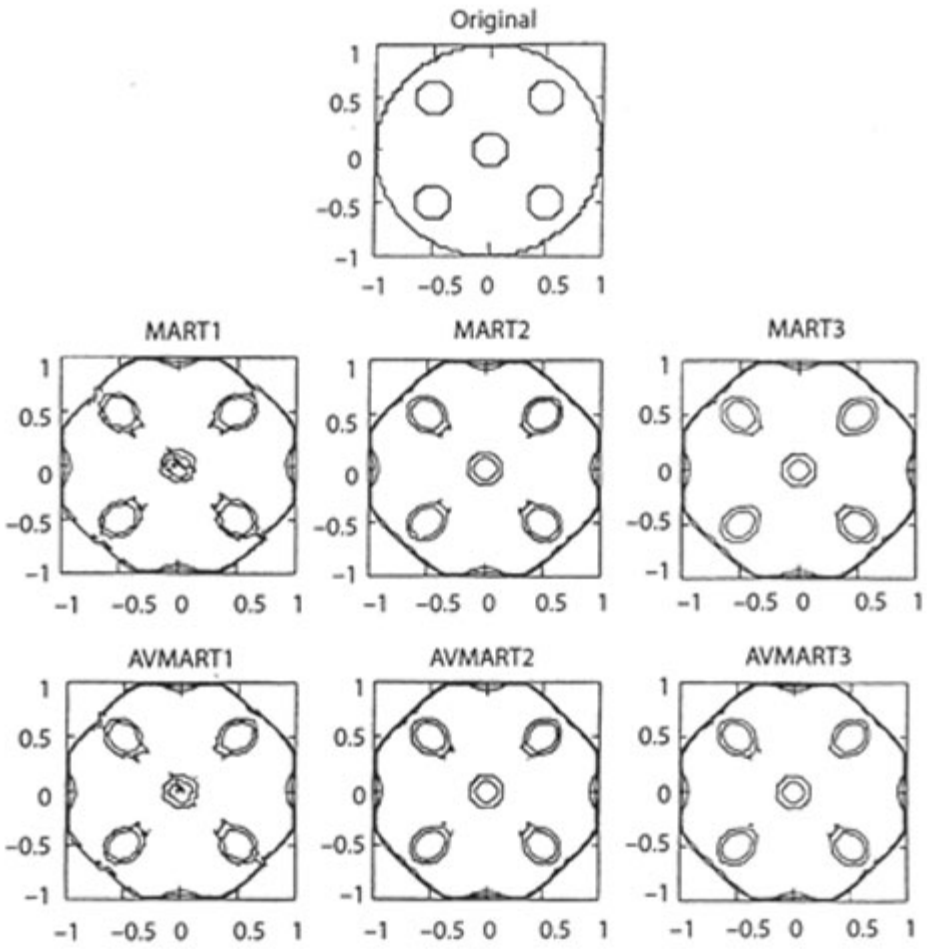

Figure 4.65: Original and Reconstructed density fields of a circular region with holes (the outer circle appears as an octago because of a finite number of view angles employed).

Previous Next

It was found that all the six algorithms reproduced a void fraction of precisely 0.34.The algorithms however different CPU time, errors, and error distribution.
The three different error norms reported in the present work are:

$$E_1 = \max\left[\text{abs}\left(\rho_{\text{orig}} - \rho_{\text{recon}}\right)\right] \text{ Maximum of absolute difference}$$

$$E_2 = \sqrt{\frac{\Sigma\left[\left(\rho_{\text{orig}} - \rho_{\text{recon}}\right)\right]^2}{N}} \text{ RMS error}$$

Table 11: Comparison of the MART Algorithms: Circular Region with Holes

Quantity	MART1	MART2	MART3	AVMART1	AVMART2	AVMART3
E_1	0.99	0.96	0.95	0.99	0.96	0.96
E_2	0.25	0.24	0.23	0.24	0.23	0.23
$E_3, \%$	25.12	24.08	23.63	24.59	23.72	23.65
Number of points (%) having error in the range						
>95%	0.27	0.05	0.05	0.27	0.05	0.05
75-95%	0.64	0.62	0.86	0.83	0.72	0.70
50-75%	3.90	4.11	4.43	3.47	4.00	3.98
Iterations	51	63	29	17	24	21
CPU (minutes)	9.51	11.97	5.65	0.32	0.45	0.40

$$E_3 = \frac{E_2}{\rho_{max} - \rho_{min}} \times 100 \text{ Noramalized RMS error, \%}$$

Results for the error level distribution in the reconstructed field have also determined. The distribution of the absolute error as a percentage of the error has been presented in the regions Errors and their distribution along with the computational details are given in Table 11.
It is clear form Table 11 that the errors for all the six algorithms are practically close, with those of MART 1 and AVMART 1 being marginally on the higher side. An examination of the error distribution shows that large error (>95%) are seen only over of the physical region shows that large errors are seen only over 27% of the physical region. Specifically, large errors are restricted to the surface of the holes, where a step change in the field property (the density in the present example) takes place. The errors are uniformly small elsewhere. The most significant difference between the original and the proposed algorithms is in terms of the number of iterations (and correspondingly in the CPU time). The proposed algorithms require less iteration for convergence and require a smaller CPU time. This is clear evidence of the computational efficiency of the proposed algorithms in the context of exact projection data.

Reconstruction of a Numerically Generated Thermal Field

The second application taken up for analysis comprises of a numerically generated convective thermal field in a horizontal differentially heated fluid layer. For definiteness, the wall temperatures employed are 15^0C and 30^0C respectively. The three-dimensional temperature field has been determined as follows. The stream function, vorticity, and energy equations are solved in two dimensions with symmetry conditions applied on the side walls, by a finite difference method [101]. The solution thus obtained corresponds to a system of longitudinal rolls spread over an infinite fluid layer. Such geometries show a polygonal plan form corresponding to a fully three-dimensional temperature field [102]. The three-dimensionality has been simulated in the present work by superimposing a sine variation in the thermal field parallel to the axis of the roll. A surface plot of the resulting temperature field revealed the flow to be organized in the form of cubic cells in the fluid layer.

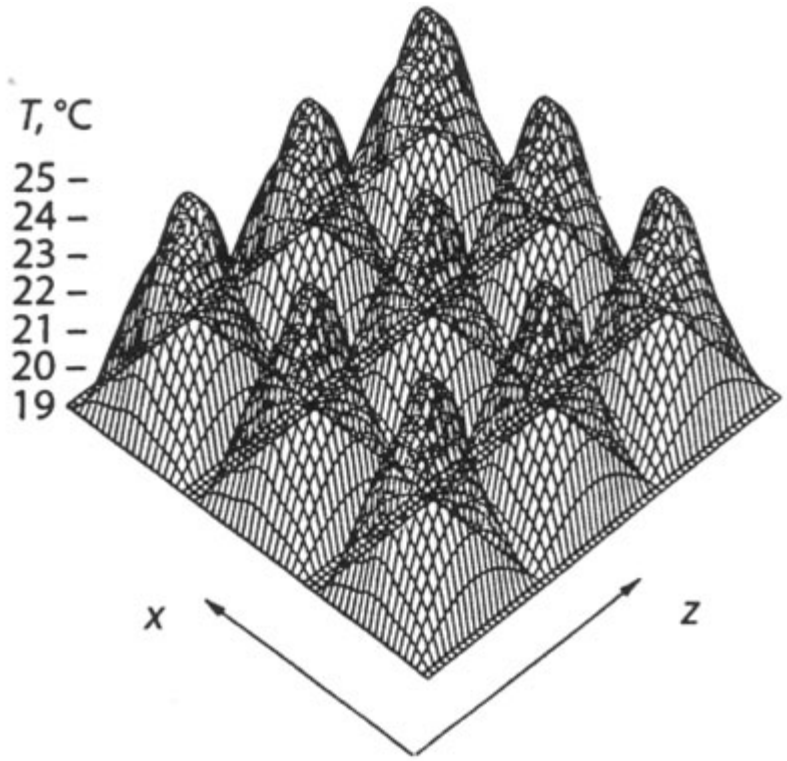

Figure 4.66: Temperature surface of the midplane of the layer, in the form of cubic cells

The advantages of selecting the field to be reconstructed in the particular manner outlined above are : (1) The field is continuous and hence reconstruction errors can be expected to be small, as compared to the application with holes.(2). Error with perfect data being small, one can systematically study errors induced by the initial guess, and noise in the projection data. (3)The thermal field begin analyzed is physically realizable.

For reconstruction, the fluid layer has been discretized into 11 planes and each plane into 61×61 cells. The relaxation factor for the proposed algorithms has been set to unity. Since the algorithms are being tested under conditions of limited data, only two and four projections have been considered. A convergence criterion of has been uniformly employed in the computation. Results obtained using the proposed MART algorithms alone have been reported.

Previous Next

The errors reported here are on the basis of the entire fluid layer. The three different errors reported are:

$$E_1 = \max\left[\text{abs}\left(T_{\text{orig}} - T_{\text{recon}}\right)\right] \ ^\circ\text{C}$$

$$E_2 = \sqrt{\frac{\sum\left[\left(T_{\text{orig}} - T_{\text{recon}}\right)\right]^2}{N}} \ \text{RMS error, } ^\circ\text{C}$$

$$E_3 = \frac{E_2}{T_{\text{hot}} - T_{\text{cold}}} \times 100 \ \text{Normalized RMS error, \%}$$

In these definitions, T_{hot} and T_{cold} are the hot and cold temperatures. T_{orig} and T_{recon} are the temperature cariables of the original and the reconstructed field respectively. Results for the error level distribution in the fluid layer have also been determined. The distribution of the absolute error as a percentage of the E_1 error has been presented in the three zones as before namely $> 95\%, 75\%$ to 95%, and $50 - 75\%$.

Table 12: Comparision of the AVMART algorithms in a Differentially Heated Fluid Layer

Initial Guess	Quantity	AVMART1	AVMART2	AVMART3
Constant	$E_1, ^\circ\text{C}$	1.97	1.97	1.97
	$E_2, ^\circ\text{C}$	0.49	0.48	0.49
	$E_3, \%$	2.86	2.79	2.86
	Iterations	9	12	14
	CPU, sec	30.6	41.3	47.2
Two-dimensional longitudinal rolls	$E_1, ^\circ\text{C}$	1.98	1.98	1.98
	$E_2, ^\circ\text{C}$	0.49	0.49	0.49
	$E_3, \%$	2.86	2.86	1.98
	Iterations	8	12	12
	CPU, sec	28.9	41.2	42.7
Random	$E_1, ^\circ\text{C}$	12.15	13.42	6.20
	$E_2, ^\circ\text{C}$	5.59	4.74	0.60
	$E_3, \%$	32.70	27.77	3.50
	Iterations	15	17	14
	CPU, sec	52.8	59.1	47.8

Previous Next

Sensitivity to Initial Guess

The inversion of matrices arising from the ART family of algorithms from limited projection data is a mathematically ill-posed problem. As a rule, the number of equations here is much smaller than the number of unknowns. This makes the solution- set infinite in the sense that a unique solution is not guaranteed. Different initial guesses, may in principle, lead to different solution of this infinite set. In the absence of any knowledge about the field being studied, it is a difficult task to prescribe the initial guess. The sensitivity of the algorithms to the initial guess has been studied with reference to three different fields, namely:

1. a constant temperature field (= $1°C$)
2. temperature distribution corresponding to two-longitudinal rolls, and
3. random field between $0°C$ and $1°C$ with an RMS value of $0.5°C$.

The guesses 1and 2 were seen to qualitatively reproduce the thermal field of figure 59 quite well(the reconstructed thermal field have not been shown as they are very close to the original). The noise present in the third guess was seen to be present in the reconstructed data. But the noise could be filtered in the frequency domain using a band-pass filter function. The reconstructed field after noise-removal was seen to be similar to the original in Figure 59. The errors, number of iterations and the CPU time for the three initial guesses are presented in Table 12.The fractional distribution of errors are reported in Table 13. With initial guesses 1and 2, the RMS and fractional of errors can be seen to be small for all the three algorithms. The maximum error is larger, but with reference to Table 13, it can be seen that large errors are restricted to small areas and are hence localized. Thus, in effect the initial guesses 1 and 2 may be considered to be equivalent. The errors corresponding to the third guess are uniformly higher for the proposed AVMART1 and AVMART2 algorithms, but small for AVMART3. The number of iterations for AVMART3are also smaller. Hence, AVMART3emertes as the best algorithm among those proposed in terms of error and CPU time for a noisy initial guess. For an unbiased and regular initial guess, computations over a wider range of parameters show AVMART2 to be the best (see the section on Sensitivity to Noise in Projection Data).

Table 13: Fractional Distribution of the E_1 Error over the fluid layer

Initial guess	Number of points (%)having error in the range	AVMART1	AVMART2	AVMART3
(1)	>95	0.17	0.17	0.17
	75-95	0.57	0.48	0.57
	50-75	5.76	5.15	5.73
(2)	>95	0.17	0.17	0.17
	75-95	0.60	0.62	0.62
	50-75	5.68	5.58	5.58
(3)	>95	0.02	0.01	0.002
	75-95	5.79	2.00	0.02
	50-75	34.46	11.92	0.30

The insensitivity of AVMART3algorithm to noise can be explained as follows , In the other two algorithms, correction is applied by finding the th root of the product of all corrections arising from ray with the cell under question. This improves the estimate of the path integral.

Previous Next

Sensitivity to Noise in projection Data

In measurements involving commercial grade optical components and recording and digitizing elements, the projection data is invariably superimposed with noise. Software operations such as interpolation and image processing can also contribute to errors in the projection data. Experience of the authors with interferometric experiments shows that the RMS noise level is around 5% [78].

The performance of the three proposed algorithms has been compared with noisy projection data as the input. A 5% noise level has been adopted for all calculations. The noise pattern has been generated using a random number generator, with a uniform probability density function. Results have been presented for 2 and 4 projections corresponding to view angles of $(0° \text{ and } 90°) \text{and } (0°, 60°, 90°, \text{and } 150°)$, respectively. The initial guess for reconstruction with 2 projections is simply a constant; for 4 projections the result obtained with 2 projections has been used as the initial guess.

Results with 2 projections show that all three algorithms reproduce qualitatively the temperature field of Figure 2. However quantitative differences are to be seen. The noise level in the reconstructed field is found to be slightly higher than that in the projection data. The magnitude of the three different errors and the distribution of the fractional error over the fluid domain are presented in Table 14. All the three algorithms are practically equivalent in terms of errors, though AVMART2 is seen to be marginally better from the error point of view. However the CPU time of AVMART1 is minimum. It is to be noted that noise (in terms of E_3) in the projection data has been amplified during the reconstruction process $(\text{from } 5\% \textit{ to } 6.4\%)$. This is in contrast to noise in the initial guess. Where iterations tend to diminish errors in the converged field.

Table 14: Comparision of the AVMART Algorithms: 5% Noise in Projection Data, Two-View Reconstruction

Quantity	AVMART1	AVMART2	AVMART3
E_1, °C	4.452	4.449	4.450
E_2, °C	1.08	1.08	1.08
E_3, %	6.37	6.36	6.37
Number of Points (%) having error int he range			
>95	0.004	0.004	0.004
75-95	0.222	0.200	0.222
50-75	4.400	4.387	4.400
Inerations	9	12	14
CPU,sec	30.5	40.9	47.8

Previous Next

Reconstruction with 4 view angles is taken up next. Table 15 shows the error levels in the reconstructed data and the distribution of this error within the fluid layer. It can be seen immediately that the errors shows that these are at best localized, i..e., large errors may occur at a few sporadic points. The AVMART1 algorithm shows a considerable deterioration in performance, since errors as well as CPU time are substantially higher. AVMART2 and AVMRT3 algorithms are seen to perform

Table 15: Comparison of the AVMART Algorithms: 5% Noise in projection data, Four-View Reconstruction

Quantity	AVMART1	AVMART2	AVMART3
E_1,°C	11.80	5.52	5.52
E_2,°C	1.78	1.36	1.36
E_3,%	10.41	8.00	8.00
Number of Points (%) having error int he range			
>95	0.004	0.007	0.007
75-95	0.029	0.349	0.346
50-75	0.276	5.186	5.177
Inerations	190	53	53
CPU,sec	1767.7	502.3	520.8

Better than AVMART1. AVMART2 is marginally superior to. AVMART3 since the error magnitudes are equal, but the former takes a smaller CPU time. Hence, a consolidated view to emerge from the discussion above is that AVMART2 exhibits the best performance.

It is of interest to compare the best proposed algorithm, namely AVMART2 with the best original MART algorithm identified by Subbarao et al. [32], Namely MART3 of the present study. To this end, reconstruction was carried out using 2-views of 0° and 90° for convection in a horizontal differentially heated fluid layer, leading to two- dimensional longitudinal rolls. The projection data was superimposed with 5% noise and an initial guess of a constant temperature field was used. Errors for MART2–new. The computer time was also higher by a factor of4 when compared with MART2_new. However the fractional distributions of errors over the fluid layer were seen to be similar for both, thus confirming that they continued to belong to the same family of algorithms.

The following inferences can now be drawn from the discussion above:

1. The three AVMART algorithms show similar performance in the presence of noise in the projection data AVMART2 is however marginally superior in terms of errors and CPU time.
2. The noise in the projection data persists after reconstruction.
3. Increasing the number of noisy projections amplifies the error in reconstruction.
4. AVMART2 clearly shows superiority over MART3 for noisy projection data. Hence it supersedes MART3 as the favored tomographic algorithm for the class of problems studied.

Both MART and AVMART algorithms have been tested extensively against experimental data. The errors as well as the convergence rates have been tested extensively against experimental data. The errors as well as the convergence rates have been reported in

Mishra et al. [81]. The conclusions drawn above carry over to experiments without any major modification. The convergence rates of all the algorithms were seen to deteriorate with increasing

number of projection angles. This could be traced to the partial de-correlation among the interferometric images owing to mild unsteadiness in the convection patterns.

Previous Next

Closure

The MART family of algorithms available in the literature was seen to require a small relaxation factor leading to delayed convergence. To address this issue, a new set of algorithms have been proposed in the present work. The new set is conceptually similar to the original, but differs significantly in the manner in which corrections are applied. Specifically, the reconstructed field does not satisfy the projection data, pointwise. However, it can accommodate a wider range of relaxation factors and thus is better from a theoretical view point. Results with the relaxation factor set at unity have been reported in the present work.

The proposed algorithms have been evaluated in the context of three applications, namely: (1)circular disk with five holes, (2) three-dimensional convective thermal field, and (3) interferometric data from a laboratory-scale differentially heated fluid layer experiment. The major results that emerge from the study are:

1. All six algorithms reconstruct the field variable in a qualitative sense. Differences are seen only in the numerical values.
2. The AVMART2 algorithm emerges as the best, in terms of CPU time, errors and sensitivity to initial guess and noise in the projection data.
3. The CPU time of the proposed algorithms is significantly; smaller than those presently available in the literature.
4. With a limited number of projections, all algorithms show large absolute maximum error, but these are sharply localize. Specifically, the qualitative appearance of the reconstructed field variable is acceptable from a practical viewpoint.
5. The convergence rate of the proposed algorithms is found to be better than the original, when the projection data is exact. In the presence of noise, all the six algo-algorithms record a sharp reduction in the convergence rate. In a few cases, the proposed algorithms require a greater number of iterations compared to the original. However, in all applications, the CPU time requirement is substantially smaller for the proposed algorithms.